applied optics

Quantification of plant morphology and leaf thickness with optical coherence tomography

Jos de Wit,[1,*] Sebastian Tonn,[2] Guido Van den Ackerveken,[2] and Jeroen Kalkman[1]

[1]Department of Imaging Physics, Delft University of Technology, Lorentzweg 1, 2628 CJ Delft, The Netherlands
[2]Plant-Microbe Interaction, Department of Biology, Utrecht University, Padualaan 8, 3584 CH Utrecht, The Netherlands
*Corresponding author: j.dewit-1@tudelft.nl

Received 1 September 2020; revised 17 October 2020; accepted 18 October 2020; posted 20 October 2020 (Doc. ID 408384); published 16 November 2020

Optical coherence tomography (OCT) can be a valuable imaging tool for in vivo and label-free digital plant phenotyping. However, for imaging leaves, air-filled cavities limit the penetration depth and reduce the image quality. Moreover, up to now quantification of leaf morphology with OCT has been done in one-dimensional or two-dimensional images only, and has often been limited to relative measurements. In this paper, we demonstrate a significant increase in OCT imaging depth and image quality by infiltrating the leaf air spaces with water. In the obtained high-quality OCT images the top and bottom surface of the leaf are digitally segmented. Moreover, high-quality en face images of the leaf are obtained from numerically flattened leaves. Segmentation in three-dimensional OCT images is used to quantify the spatially resolved leaf thickness. Based on a segmented leaf image, the refractive index of an infiltrated leaf is measured to be 1.345 ± 0.004, deviating only 1.2% from that of pure water. Using the refractive index and a correction for refraction effects at the air-leaf interface, we quantitatively mapped the leaf thickness. The results show that OCT is an efficient and promising technique for quantitative phenotyping on leaf and tissue level.

https://doi.org/10.1364/AO.408384

1. INTRODUCTION

With an increasing world population and growing biofuel consumption, the demand for crops is expected to increase rapidly over the coming decades [1]. Plant scientists use methods such as crop monitoring, environment control, early disease detection, and plant breeding to improve both the quality and quantity of food production. Plant phenotyping, i.e., the evaluation of the performance and appearance of a plant in its environment, is a crucial step in the development and optimization of these methods. Traditional phenotyping, i.e., scoring of plants by human raters based on visual inspection, is more and more replaced by digital phenotyping, which aims to objectively and quickly quantify relevant plant traits at low cost [2]. Imaging and computer vision approaches play a central role in digital phenotyping. While many studies focus on high-throughput phenotyping with limited resolution and dimensionality, the long-term goal is for three-dimensional (3D) high-resolution phenotyping for a deeper comprehension of plant phenotypes [3]. In this paper, we show how optical coherence tomography (OCT) can contribute to plant trait quantification in high-resolution phenotyping.

Leaves are the plant's organs where sunlight is captured and carbohydrates are synthesized, making them an important object for high-resolution plant phenotyping on organ, tissue, and cellular scales [3]. Microscopic phenotyping of plant leaves often needs fixation, clearing, and staining, especially when the deeper mesophyll layer and vascular tissue are investigated [4,5]. Such extensive sample preparation not only reduces phenotyping throughput, but also makes it impossible to do longitudinal in vivo measurements. Longitudinal measurements, i.e., following the same tissue in time, are important to study leaf dynamics such as leaf growth and plant interaction with the environment [6,7].

Tomographic methods such as magnetic resonance imaging (MRI) and high-resolution X-ray computed tomography (HRXCT) are able to obtain 3D images of leaf morphology in vivo at resolutions of typically 30 μm for MRI and 10 μm for HRXCT [8]. The drawbacks of these computed tomographic methods are their low speed and high cost [9], as well as the trade-off between sample size and resolution [8].

OCT is developed for label-free in vivo imaging deep into scattering biological tissue [10]. OCT has been used to obtain 3D images of plants with resolutions between 5 and 10 μm. Due

to the combination of confocal gating and coherence gating, multiply scattered light is largely filtered out and the penetration depth becomes many times that of confocal microscopy. It has been used to reveal plant anatomy [11,12], detect plant diseases [13–17], study leaf senescence [18], and investigate root growth dynamics [19]. Moreover, OCT is used in post-harvest quality evaluation of agriculture produce [20].

Most OCT studies on (early) disease detection have compared A-scans that were obtained by laterally averaging flattened B-scans [13–16]. Pathogen-induced cell degradation results in a broadening of, or a changing distance between, peaks in the average A-scan. This has been successfully used as a bio-marker for plant diseases. Wijesinghe et al. quantified the average thickness of the palisade parenchyma layer by dividing the optical path length (OPL) between the two peaks in the average A-scan through an assumed leaf refractive index [14,15]. Other studies have described changes in the average A-scan in a mere qualitative way. Chow et al. used scattering intensity as a measure for disease infection, but the values were given in arbitrary units and are hence not transferable between setups [17]. Anna et al. measured the attenuation coefficient of leaves as an indicator of senescence [18]. Additionally, they calculated texture parameters of gray level B-scans to quantitatively classify different stages of senescence.

However, all these studies demonstrate two major drawbacks. First, none of these studies were able to clearly visualize the entire cross-section of a mature leaf, including the opposite leaf surface, due to a limited penetration depth. Even if signals are picked up from deeper regions, the signals that have a low signal-to-noise ratio (SNR) are further deteriorated due to multiply scattered photons and sample-induced aberrations. The relatively low penetration depth as compared to other biological tissues is caused by the fact that leaves contain air-filled cavities. At these air-tissue interfaces, strong scattering and refraction occur, giving rise to the multiply scattered signal and sample-induced aberrations [21]. This effect can be largely reduced by infiltrating the leaves with a liquid that has a refractive index close to that of the leaf tissue. Infiltration of leaves with perfluorodecalin (PFD) has been used to enhance the resolution and image quality in in vivo confocal microscopy [22]. PFD has a low surface tension and thus infiltrates easily into the leaf even under atmospheric pressure. Infiltration with PFD is done by soaking the leaves for 5 min in the solution [23], which is difficult to apply on leaves still on the plant. Water also can be infiltrated into leaves by pressing the opening of a water-filled syringe against the abaxial leaf epidermis and applying gentle pressure, or by releasing air from leaves held underwater using a vacuum pump allowing water to enter after the vacuum is gently released [24]. Syringe-based water infiltration takes a few seconds and the infiltrated leaves dry within an hour, returning the leaf to its normal state. Moreover, water is available everywhere, significantly cheaper than PFD, and part of the natural environment of plants. Both PFD and water are believed to have marginal physiological effects and thus infiltration with these liquids is feasible with in vivo imaging [22].

Second, the mentioned publications did not show quantification of 3D leaf morphology and layer thickness. Current leaf quantification often yields relative values that cannot be translated into objective physical quantities. For example, the measured OPL was not always transformed into physical thickness, and if done, a literature value for water or plant cells was used. Moreover, most quantification was based on laterally averaged A-scans that do not capture the full 3D shape. This is mainly because of a lack of application of advanced image processing and segmentation.

A particular morphological feature that is of interest is leaf thickness, which can be important, for example, to accurately determine a plant's biomass [25]. The current methods to measure lateral resolved leaf thickness require extensive clearing [5], complex and costly equipment [25], or a custom-build complex setup [26], or give no accurate results [27]. OCT can be an attractive alternative method to measure leaf thickness, especially when combined with a study of the internal leaf tissue morphology.

In this paper, we address the problems of limited penetration depth and lack of quantification of 3D morphology in current OCT plant imaging. First, we demonstrate that water infiltration successfully extends the penetration depth and gives higher-quality images. Second, we use these higher-quality images in combination with image processing and segmentation to quantify lateral resolved leaf thickness. Compared to alternative methods, OCT is a simple and cost-efficient tool for measuring lateral resolved leaf thickness.

2. METHODS

A. Experimental OCT Setup

The measurements are performed with a high-resolution spectral-domain OCT setup (Ganymede II HR, Thorlabs, Germany) that has a super-luminescent diode light source with a center wavelength of 900 nm and a full width half maximum (FWHM) bandwidth of 120 nm. The axial resolution is experimentally measured to be 3.0 μm in air, which corresponds to 2.2 μm in tissue. The spectrometer covers a bandwidth of 220 nm over 2048 pixels, giving a spectral sampling resolution of 0.11 nm and an axial imaging range of 1.87 mm in air. The system is operated with an A-scan rate of 36 kHz, enabling real-time acquisition of B-scans and sub-minute acquisition of volume scans. The objective lens (OCT-LK4-BB, Thorlabs, Germany) has a working distance of 41.6 mm and a maximum lateral field of view of 16mm × 16 mm, though in this research smaller scan areas were used to reduce the memory usage. The lateral resolution is experimentally determined with a knife-edge imaging a step response to have a FWHM of 6 μm. The raw spectral data is obtained with ThorImage software (version 5.2.0). The B-scans consist of 1024 A-scan lines over a width of 3 mm in x-direction, corresponding to a scan line every 3 μm. Every A-scan is averaged eight times to improve the SNR). The 3D scans consist of 512 × 512 scan lines over an area of 3 × 3 mm^2. The resulting separation of 6 μm between the scan lines corresponds well to the lateral resolution resulting in a well-sampled volume. One of the limitations of volume OCT imaging is the size of the data sets that are created. For the 3D acquisition with 2048 pixels per A-scan and 2 bytes per pixel (for 12 bit numbers), the raw spectral data has a size of 1 GB. To limit the data size, only two averages per A-line are made, giving a raw spectral data size of 2 GB. The scan time of 512 × 512 × 2 A-scans is 15 s, which gives no practical limitation for application in plant imaging.

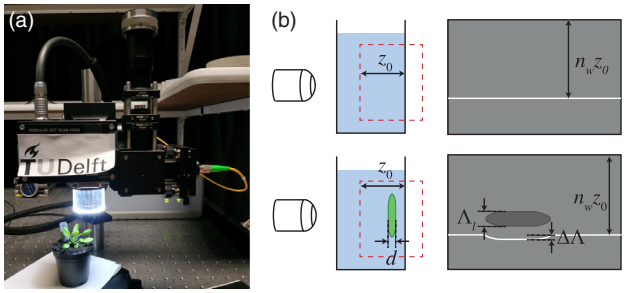

Fig. 1. SD-OCT setup that was used for this study. (a) The setup in action. (b) A schematic overview of the refractive index measurement. The red dashed boxes indicate the area of the image. z_0 and d are physical distances, while Λ is the distance in OPL.

The raw spectral data is processed in Python 3 to obtain high-quality images. The processing consists of subsequently the subtraction of the reference spectrum, interpolation to an equally spaced grid in wavenumber domain, apodization with a Hanning window, correction for dispersion mismatch, and an inverse discrete Fourier transform. The numerical correction for the dispersion mismatch between the reference and sample arm is done with a fourth-order polynomial, whose coefficients are obtained from a reference measurement of a single reflector [28]. After processing, the A-scans belonging to the same scan line are complex averaged to improve the SNR [29]. For segmentation, the absolute value of the complex averaged scan lines is used directly. For displaying in images, this amplitude is subsequently converted to a dB scale by dividing through the maximum, taking the 10-base logarithm, and multiplying by 20.

B. Plant Material

Measurements are taken on a fully developed leaf of a mature four-week-old Arabidopsis plant of accession C24 [30]. The leaf is infiltrated by pressing the mouth of a syringe to the abaxial side of the leaf and gently pushing the water into the leaf until it is completely infiltrated, visible because of the induced translucence. The infiltrated leaf dries within an hour and the physiological effects of infiltration on the leaf are minimal. After drying, the area of infiltration is not recognizable by the naked eye, nor in the OCT scan. This allows for in vivo imaging of the same area of a leaf longitudinal, i.e., at different times during growth. The OCT measurements are taken from the adaxial (top) side of the leaf. The leaf can remain on the plant, as the whole plant is placed below the scan head, as shown in Fig. 1(a). The sample is placed below the zero-delay with an extra offset to separate the image from auto-correlation artifacts.

C. Surface Segmentation

For quantitative analysis of the morphological traits of plant leaves, the location of the top surface and bottom surface of the leaf are segmented.

The segmentation starts with an OCT cross-sectional image [Fig. 2(a)], where the signal from the entire leaf is well above the noise level. Thresholding is applied to obtain a rough segmentation of the leaf. The threshold is taken sufficiently low to capture the weaker reflections from the bottom surface and the places

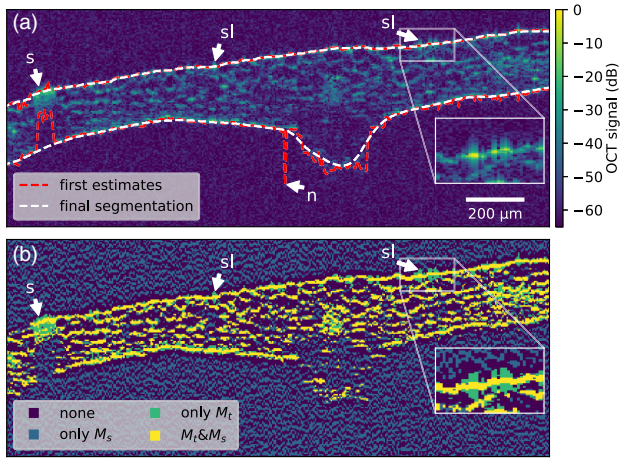

Fig. 2. Illustration of the steps in surface segmentation to obtain leaf thickness. (a) Cross-sectional OCT image and the results of the two steps in image segmentation. (b) Segmentations resulting from thresholding (M_t, green), from taking a negative second derivative (M_s, light blue) and the overlap of both (yellow). The arrows point to a soil particle (s), side lobes of the top reflection (sl), and noise above the threshold (n).

where the local normal of the top surface of the leaf is tilted with respect to the optical axis. This results in the segmentation M_s, as shown in yellow and green in Fig. 2(b).

The segmentation by thresholding includes many high-intensity side lobes, visible as the light green lobes on the surface in Fig. 2(b), annotated with arrow sl. To remove these side lobes, an additional requirement is imposed that the second-order Gaussian derivative ($\sigma = 3$ pixels) along the axial direction should be negative. This negative second derivative filter (M_s, light blue and yellow) effectively acts as a local maximum filter, discarding the band before the peak positions of the top and bottom surface. It successfully removes the side lobes and increases the accuracy of the segmentation of mainly the top surface.

Subsequently, the first and last non zero pixels for each A-scan in this segmentation are taken as the first estimates for the top and bottom surface, respectively, indicated with the red line in Fig. 2(a). Higher-intensity noise (indicated with n) and structures like leaf hairs or small soil particles (indicated with s) result in outliers in these first surface estimates. To remove the outliers a median filter is applied with a 7 pixel radius circular footprint. After median filtering, the bottom surface is smoothed by a Gaussian kernel with a sigma of five pixels. These filters result in a smooth and accurate segmentation for the top and bottom surface, as indicated by the white dashed line. Implemented with Python operating in Spyder on a desktop (Intel Xeon W-2223 CPU), the surface segmentation of the 512×512 scan lines volume took 24 s, of which 15 s were spent on calculating the Gaussian derivative filtered image.

D. Leaf Refractive Index Measurement

OCT measures axial distances in optical path length (OPL). Conversion between the OPL and the depth is done by dividing through the refractive index of the medium, in this case, the refractive index of infiltrated leaf tissue.

We quantify the refractive index of an infiltrated leaf with a method similar to the in vitro method of Tearney *et al.* [31]. A water-filled cuvette is imaged twice: first with the leaf placed in a cuvette close to the back surface, then after the leaf is removed while the probe and cuvette remain in their position, as shown in Fig. 1(b). The displacement of the wall of the cuvette between the two OCT images is equal to the difference in the OPL between light going through the leaf tissue and light going through water. The relative difference of the refractive index can be calculated for each lateral position with

$$\frac{n_l - n_w}{n_w} = \frac{\Delta\Lambda}{\Lambda_l - \Delta\Lambda}, \tag{1}$$

where n_l and n_w are the refractive indices of respectively an infiltrated leaf and water, respectively; Λ_l is the thickness of the leaf in OPL; and $\Delta\Lambda$ is the displacement of the cuvette wall in OPL, as indicated in Fig. 1(b). Although this method does not account for refraction at the leaf surface, the resulting error will be insignificant as the difference in the refractive index is expected to be small. For fully automated refractive index measurement, both the leaf and cuvette surface are segmented. Λ_l is obtained from the surface segmentation, as described in Section C. The location of the cuvette wall is obtained for each A-scan by fitting a Gaussian to a manually selected 100 μm wide axial region around the cuvette wall. The obtained peak locations are subsequently median filtered with a 25 pixel window to remove outliers, and then Gaussian filtered with a sigma of 15 pixels to obtain a smooth curve. For each lateral position equation Eq. (1) is evaluated. The final refractive index is obtained by averaging over all lateral positions.

E. Leaf Thickness Measurement

For each lateral position, the distance in the OPL between the top and bottom surface is divided by n_l to obtain the physical distance l between the top and bottom surface. This distance l is measured along the beam path; thus it will be larger than the leaf thickness d for an oblique leaf surface, as indicated in Fig. 3. Taking refraction into account and assuming that the leaf can locally be considered as having two parallel surfaces, the true leaf thickness d can be obtained with

$$d = l\sqrt{1 - \left(\frac{\sin\theta_i}{n_l}\right)^2}, \tag{2}$$

where d is the local thickness measured perpendicular to the top surface, l is the local thickness measured as the distance in the A-scan between the top and bottom reflection, θ_i is the angle of the leaf surface with respect to the optical axis, and n_l is the leaf refractive index, as shown in Fig. 3(a). Figure 3(b) shows the values of the correction factor d/l for incident angles up to 45°. The local θ_i is calculated by taking the inverse tangent of the Gaussian gradient magnitude of the top surface with a sigma of 10 pixels (60 μm). The leaf thickness d is calculated with Eq. (2).

F. En face OCT Images

With the segmented top surface en face images at a fixed depth below the top surface are made. The leaf in the C-scan is numerically flattened by shifting the leaf top surface to the first pixel for each A-scan. From each depth of interest, a slice in the transverse direction is taken and displayed as an en face image. The reference intensity for conversion to the dB scale is the maximum value of the entire data set.

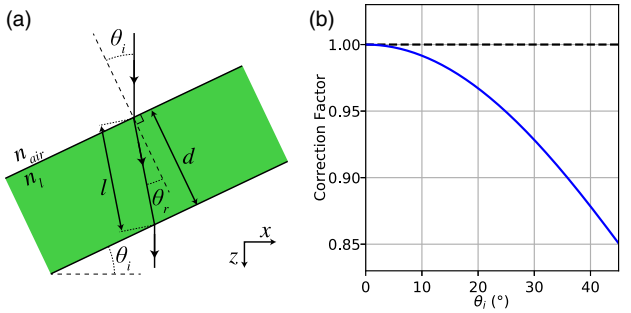

Fig. 3. (a) Geometry and parameters for calculating the correction factor. The scan beam falls in the vertical direction and the leaf is tilted with an angle θ_i with respect to the horizontal. x and z are the horizontal and vertical coordinates in the images, respectively. (b) The correction factors for leaf tilting angles θ_i between 0° and 45°, using $n_l = 1.345$.

3. RESULTS

A. Result of Leaf Infiltration on the OCT Imaging Depth

Figure 4 shows an image of the same leaf before and after infiltration. The images are not taken from exactly the same position as the plant moved during infiltration. In both images, the adaxial epidermal cells are clearly visible, as are the mesophyll cells just below the epidermal cells. At some places, the strong reflections from the air-leaf interface give side lobes that partly obscure the epidermal cells. Without infiltration, the image gets blurry after penetration of about 100 μm OPL. As this leaf is relatively thin, the abaxial side can be seen from a drop of intensity after about 200 μm OPL, but the transition is rather vague and its location far from precise. Moreover, the B-scan area crosses the midrib around the center of the image, but this is not visible in the image.

The relatively poor image quality in the deeper regions of the non-infiltrated leaf can be understood from the presence of air-filled cavities that the plant uses for gas exchange. These cavities with a refractive index that is much lower than that of leaf tissue cause aberrations and refraction of the beam such that the back-reflected signals are disturbed and, if collected, mapped to the wrong location. The many air-tissue interfaces also cause a lot of multiple scattering, which further decreases the visibility of deeper-lying structures in the leaf. Multiple scattering also gives rise to the haze, visible at the bottom of the leaf, which corresponds to the longer path lengths of multiply scattered light [32]. This further obscures the abaxial leaf surface in the image.

Filling these cavities with water by infiltrating the leaves makes them much more transparent to the OCT signal, thereby reducing sample-induced aberrations and multiple scattering. In Fig. 4(b), cells are visible in the deeper regions of the cell, and also the vascular tissue in the midrib can be clearly distinguished.

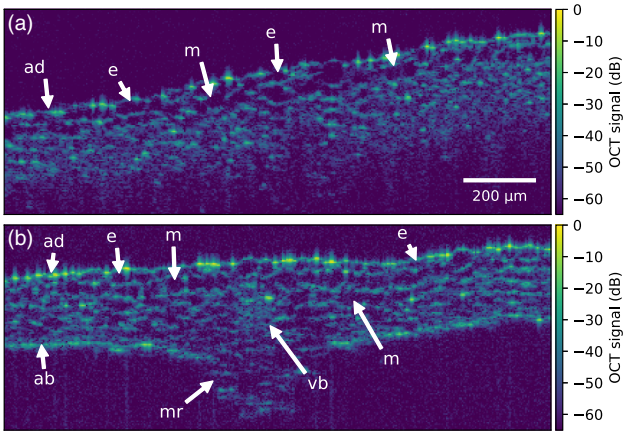

Fig. 4. B-scan images of the central part of an Arabidopsis leaf. (a) An image before infiltration and (b) an image after infiltration. The scan area of (a) crosses the midrib about halfway in the image. In (b) the midrib and vascular tissue are clearly visible. In contrast to (a), the abaxial side of the leaf is clearly visible in (b). e, epidermal cell; m, mesophyll cell; vb, vascular bundle; mr, midrib; ad, adaxial side; ab, abaxial side.

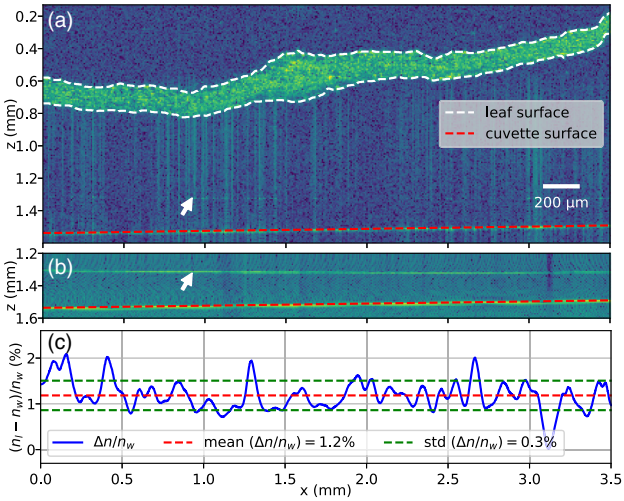

Fig. 5. (a) B-scan image of an infiltrated leaf in a cuvette and (b) the image after the leaf has been removed while the setup and cuvette remained untouched. From the segmentation of the leaf surface and the cuvette surface, the relative refractive index difference is calculated per lateral position using Eq. (1) and plotted in (c). The mean relative difference $\overline{\Delta n/n_w}$ is indicated by the red dashed line, and the green dashed lines indicate the single standard deviation borders.

The clearest difference between the images is that with infiltration the abaxial side of the leaf is clearly and accurately imaged. Moreover, the shape of the midrib on the abaxial side can be clearly distinguished. The comparison of these images shows the huge benefit of infiltration for OCT imaging of plant leaves, making it possible to clearly image the full cross-section of the leaf in vivo, and also quantifying leaf thickness as a function of lateral position. We will explore the latter in the next subsection.

B. Leaf Refractive Index Measurement

Figures 5(a) and 5(b) show a B-scan of a water-filled cuvette with and without an infiltrated leaf. The white arrows point to an auto-correlation artifact of the cuvette wall, which is sufficiently separated from the relevant features to enable accurate segmentation. The vertical stripes in the images are probably caused by aliasing of reflections of a surface of the cuvette outside the axial range. These artifacts, however, do not cause any problems in the segmentation as their intensity is well below the intensity of the leaf and the cuvette wall. The segmented leaf and cuvette surface are indicated with a white and a red dashed line, respectively. The average difference in the OPL of the cuvette $\overline{\Delta\Lambda} = 2$ µm, which corresponds to one pixel. For each lateral position equation, Eq. (1) is evaluated and the result of it plotted in Fig. 5(c). The average relative difference in the refractive index between infiltrated leaf tissue and water is 1.2%. This relative difference is small enough to justify the neglect of refraction at the leaf surface. Using the literature value $n_w = 1.329$ at the center wavelength of the OCT setup ($\lambda_c = 900$ mm) [33], we obtain a refractive index for infiltrated leaf tissue of $n_l = 1.345 \pm 0.004$. The variation in the measured refractive index is caused by a combination of uncertainty in both measurement and segmentation, and the natural variation of leaf tissue.

C. Leaf Thickness

The leaf thickness is determined for a section of the leaf around the midrib, indicated with the red box in Fig. 6(a). Figure 6(b) shows the segmented top and bottom surface in 3D. The midrib is clearly visible in the segmentation of the bottom surface. The peak at the right side is an artifact caused by the presence of a trichome (a leaf hair). The correction factor d/l as defined by Eq. (2) is evaluated and visualized in Fig. 6(c). For the major part of the surface, this factor is close to 1; at the lower half of the image, it decreases to values down to 0.93 due to the slope of the surface. Around the leaf hair, the gradient magnitude becomes much larger, resulting in local correction factors up to 0.83. From the segmentation, the correction factor, and the measured refractive index $n_l = 1.345$, the lateral resolved leaf thickness is determined and visualized in Fig. 6(d). The midrib is clearly visible due to its large thickness ranging from 260 µm at the right to 366 µm at the left of the image. Moreover, the veins can be distinguished with a thickness of around 180 µm, while the lamina or leaf blade has a thickness varying between 110 µm and 150 µm. Two artifacts, caused by a soil particle and a leaf hair, are indicated with arrows.

D. En Face Images

Using the surface segmentation, en face images are obtained at different depths with respect to the top surface of the leaf. This is shown in the single OCT cross-section in Fig. 7(a), with the lines indicating the depths in the OPL of the en face images (b–f). In the cross-sectional image, the vascular bundle inside the midrib is clearly visible and has a diameter of about 120 µm.

The first layer [Fig. 7(b)] corresponds to the cuticle and the top of the epidermal cells. The air-tissue interface gives strong reflections, resulting in high intensities in this image. The structure in the image is an indication of the local orientation of the

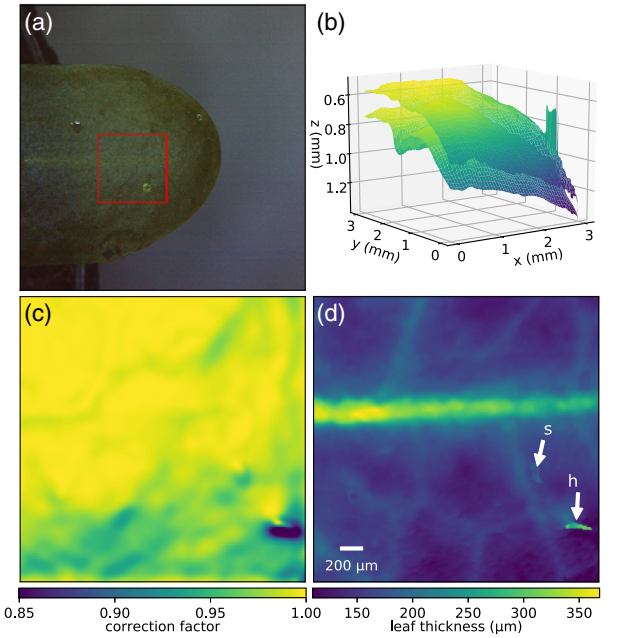

Fig. 6. (a) RGB image with the scan region indicated by the red box. (b) The segmented top and bottom surface. (c) The correction factor for tilted surfaces taking refraction into account. (d) The lateral resolved leaf thickness assuming $n_l = 1.345$. The arrows indicate small artifacts in the segmentation due to a soil particle (s) and a leaf hair (h). The leaf hair is visible as the peak on the right side of (b).

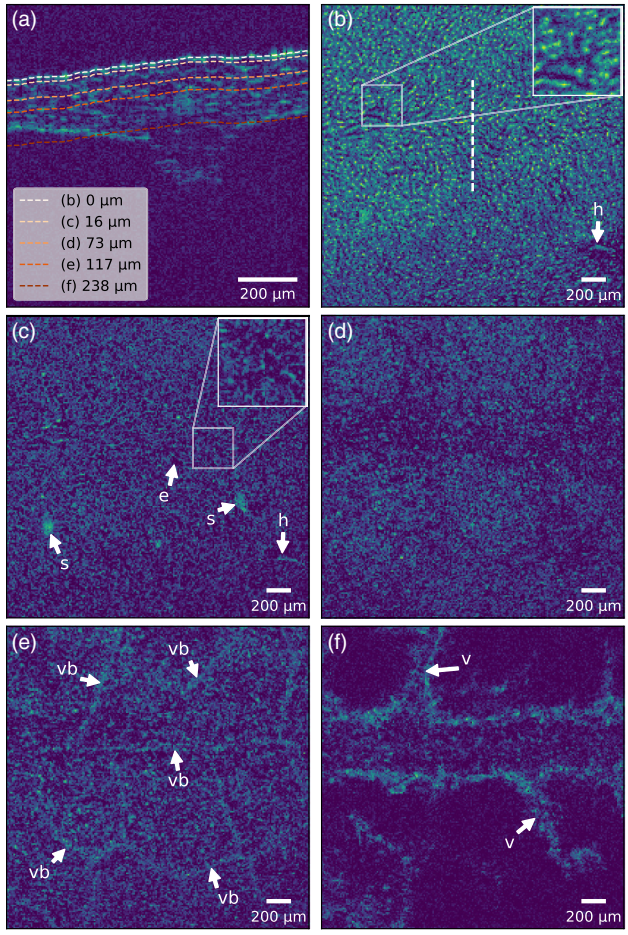

Fig. 7. En face images of the leaf at a fixed distance in OPL from the adaxial surface, generated from the same data that is used in Fig. 6. The lines in (a) indicate the depth of the images in (b)–(f). (b) OCT surface intensity showing the cuticle and the top surface of the epidermal cells. The white dashed line indicates the location of the cross-section (a). (c) The image at 16 µm depth, which is located in the epidermal layer. (d) The image at 73 µm depth, which is located in the palisade mesophyll layer. (e) The image at 117 µm, showing the vascular bundles of the midrib and veins, and the spongy mesophyll layer between the veins. Several vascular bundles are annotated. (f) The image at 238 µm, which is below the leaf at the lamina or leaf blade, while it still contains tissue around the midrib and leaf veins. All images are plotted on a scale between 0 and −65 dB, where 0 refers to the maximum value in the 3D data set. The distance from the surface and z in (a) are given in OPL. e, epidermal cell; h, leaf hair; s, soil particle; vb, vascular bundle; v, vein.

leaf surface. A surface normal along the axis of the OCT beam gives a high-intensity signal back on the detector. The reflected intensity decreases with an increasing angle. The bottom 0.5 mm area has a lower average intensity as the leaf surface is sloped downward there. In the right bottom, a leaf hair is visible, which caused an artifact in the top surface segmentation. Figure 7(c) is located at the epidermal layer, and indeed many epidermal cells can be distinguished, and are better visible in the inset. The typical width of the lobes of the cells is 40 to 50 µm. Two bright dots contain the high-intensity reflections from grains of soil, and also the leaf hair is still visible. The epidermal cells are less well visible in the lower part, probably due to the sloped surface. Figure 7(d) shows the palisade mesophyll layer, and has a distinctly different texture than the epidermal layer. The lateral size of the cells is smaller, typical 20–30 µm, giving a finer texture. This layer has a more open structure at the midrib and also at some of the larger veins. When we go deeper to 117 µm (OPL) into the leaf, the vascular bundles can be seen in the midrib and the veins. The location of these vascular bundles corresponds well with the location of veins in Fig. 6(d). The mesophyll cells in the lamina areas look slightly more open than those in Figure 7(d). This indicates that this slice is indeed through the spongy mesophyll with many cavities for gas exchange, and that the one in (d) is located in the palisade mesophyll layer. The cavities have an irregular structure, but the width along their smallest dimension is typically 50–70 µm, and up to 90 µm close to the midrib. When taking a slice below the bottom surface of the lamina regions, the veins and the thicker leaf at the edges of the midrib are clearly visible. The signal at the right bottom is due to a locally thicker surface, as can be seen in Fig. 6(b). Cross-section images show that this thickening appears at both the top and the bottom, which may be related to the leaf hair that is in its vicinity.

4. DISCUSSION

This work presents water infiltration as a method to increase the OCT imaging depth and image quality of plant leaves. In addition, we show quantification of the refractive index of leaves and the lateral resolved leaf thickness.

The key advantages of OCT for quantifying lateral resolved leaf thickness are that it is fast, minimally invasive, and compatible with label-free in vivo imaging, and that it gives leaf

thickness and internal leaf morphology at once at a relatively low cost using commercially available systems. The results presented in this paper show that OCT can be successfully used to quantify spatially resolved leaf thickness and that it provides further insight into the underlying leaf morphology.

A disadvantage of our method is that infiltration locally changes the leaf environment. As water is added to the leaf, this method may be less suitable for longitudinal drought monitoring studies. However, when the time between measurements is longer than the drying time of the leaf, the physiological effects of infiltration will probably be limited. Based on the presented results, it cannot be excluded that infiltration has any effect on the leaf thickness. However, this effect will be less than with optical clearing and the same for different plants or leaf areas. Therefore, it will barely limit the applicability for plant studies. Syringe infiltration sometimes bruises the leaf on the small ring where the syringe mouth is pressed on the leaf. This can be avoided by using a vacuum pump or PFD infiltration, which is expected to give similar imaging results.

Sample-induced beam deviation and systematic errors in the segmentation may be a source for systematic errors or inaccuracy of the leaf thickness measurement. Therefore, the proposed method to compensate for beam refraction is essential to obtain an accurate result with an oblique leaf surface. Even with this method, the limited axial imaging range and the possibility of image warping still require the orientation of the leaves to be as close to horizontal as possible.

The accuracy of the leaf thickness quantification depends on the quality of the surface segmentation. In this work, we present a simple but robust segmentation method that gives good results, excluding side lobes at the top surface that would otherwise have caused a systematic error toward a thicker surface. Structures on the surface, like leaf hairs, cause errors in the segmentation. These artifacts can be removed by more aggressive filtering, at the expense of losing spatial detail. Smaller leaf hairs, of plants such as tomato or lettuce, will be largely filtered out by the proposed median filter. Moreover, leaf hairs can be a relevant feature of a plant's phenotype, and OCT is very suitable to quantify both their surface density and 3D shape. The speed and accuracy of the segmentation may be improved by applying more advanced segmentation methods, for example, those based on deep learning.

Our approach can also be applied to other plant species with different leaf sizes. Using syringe infiltration, we successfully imaged full cross-sections, including the bottom surface, of lettuce, tomato, dandelion and ribwort plantain leaves. However, plant leaves with many fibers, such as willow or reed leaves, were difficult to infiltrate with a syringe. Moreover, the attenuation of these leaves is higher. Therefore, our method worked less well for such leaves. We obtained the best imaging results with fresh and green leaves, where we were able to image full cross-sections for leaf thicknesses up to 350 μm.

For very thick or highly scattering leaves, infiltration may not give enough of an increase in penetration depth to accurately image the other side of the leaf. The penetration depth can be increased by using an OCT system with a larger center wavelength, at the expense of a lower imaging resolution. Dual-side view OCT (DSV-OCT) can be used to measure the lateral resolved thickness of opaque objects, and thus even of non-infiltrated leaves [34]. Compared to the dual confocal laser profiler [26], DSV-OCT also gives an image of the internal leaf morphology by fusing the images from both sides. However, it has the same disadvantages as the dual confocal laser profiler, namely, it is a custom-build, complex setup and needs close access to both sides of the leaf.

Our OCT images have the potential for quantifying many more morphological features, such as individual cells and vascular bundles. Segmentation methods to extract such features from 3D confocal microscopy images [35–37] can be adapted for use on OCT plant images. This may enable further quantification of plant leaf morphology and dynamics. Moreover, our leaf thickness measurements can be applied to larger-scale plant studies. Those studies include imaging on whole leaves and comparing leaf thickness of different varieties, and longitudinal studies on the development of leaf thickness during plant growth. Hence, we foresee a great potential of our technique for quantification of 3D leaf morphology in digital phenotyping.

5. CONCLUSION

With this work, we show that water infiltration of plant leaves significantly improves the penetration depth and image quality for OCT plant imaging. With water infiltration, we imaged entire cross-sections of plant leaves, measured their refractive index, and successfully quantified the lateral resolved leaf thickness with high accuracy.

Data Availability.

Data sets and analysis code is available at the Zenodo repository, accessible via the DOI: 10.5281/zenodo.4059559.

Funding. Nederlandse Organisatie voor Wetenschappelijk Onderzoek (16293).

Disclosures. The authors declare no conflicts of interest.

REFERENCES

1. D. K. Ray, N. D. Mueller, P. C. West, and J. A. Foley, "Yield trends are insufficient to double global crop production by 2050," PLoS ONE **8**, e66428 (2013).
2. F. Fiorani and U. Schurr, "Future scenarios for plant phenotyping," Annu. Rev. Plant Biol.**64**, 267–291 (2013).
3. S. Dhondt, N. Wuyts, and D. Inzé, "Cell to whole-plant phenotyping: the best is yet to come," Trends Plant Sci. **18**, 428 (2013).
4. N. Wuyts, J.-C. Palauqui, G. Conejero, J.-L. Verdeil, C. Granier, and C. Massonnet, "High-contrast three-dimensional imaging of the *Arabidopsis* leaf enables the analysis of cell dimensions in the epidermis and mesophyll," Plant Meth. **6**, 17 (2010).
5. N. Wuyts, C. Massonnet, M. Dauzat, and C. Granier, "Structural assessment of the impact of environmental constraints on *Arabidopsis thaliana* leaf growth: a 3D approach," Plant Cell Environ.**35**, 1631–1646 (2012).
6. L. Remmler and A.-G. Rolland-Lagan, "Computational method for quantifying growth patterns at the adaxial leaf surface in three dimensions," Plant Physiol.**159**, 27 (2012).
7. A. Walter, W. K. Silk, and U. Schurr, "Environmental effects on spatial and temporal patterns of leaf and root growth," Annu. Rev. Plant Biol.**60**, 279–304 (2009).
8. S. Dhondt, H. Vanhaeren, D. Van Loo, V. Cnudde, and D. Inzé, "Plant structure visualization by high-resolution X-ray computed tomography," Trends Plant Sci. **15**, 419 (2010).

9. L. Li, Q. Zhang, and D. Huang, "A review of imaging techniques for plant phenotyping," Sensors**14**, 20078–20111 (2014).
10. D. Huang, E. Swanson, C. Lin, J. Schuman, W. Stinson, W. Chang, M. Hee, T. Flotte, K. Gregory, C. Puliafito, and J. Fujimoto, "Optical coherence tomography," Science**254**, 1178–1181 (1991).
11. J. W. Hettinger, M. d. L. P. Mattozzi, W. R. Myers, M. E. Williams, A. Reeves, R. L. Parsons, R. C. Haskell, D. C. Petersen, R. Wang, and J. I. Medford, "Optical coherence microscopy. A technology for rapid, in vivo, non-destructive visualization of plants and plant cells," Plant Physiol. **123**, 3 (2000).
12. A. Reeves, R. L. Parsons, J. W. Hettinger, and J. I. Medford, "*In vivo* three-dimensional imaging of plants with optical coherence microscopy," J. Microsc.**208**, 177–189 (2002).
13. M. Boccara, W. Schwartz, E. Guiot, G. Vidal, R. D. Paepe, A. Dubois, and A.-C. Boccara, "Early chloroplastic alterations analysed by optical coherence tomography during a harpin-induced hypersensitive response," The Plant J. **50**, 338–346 (2007).
14. R. Wijesinghe, S.-Y. Lee, P. Kim, H.-Y. Jung, M. Jeon, and J. Kim, "Optical inspection and morphological analysis of *Diospyros kaki* plant leaves for the detection of circular leaf spot disease," Sensors**16**, 1282 (2016).
15. R. E. Wijesinghe, S.-Y. Lee, N. K. Ravichandran, S. Han, H. Jeong, Y. Han, H.-Y. Jung, P. Kim, M. Jeon, and J. Kim, "Optical coherence tomography-integrated, wearable (backpack-type), compact diagnostic imaging modality for *in situ* leaf quality assessment," Appl. Opt.**56**, D108–D114 (2017).
16. A. Rateria, M. Mohan, K. Mukhopadhyay, and R. Poddar, "Investigation of *Puccinia triticina* contagion on wheat leaves using swept source optical coherence tomography," Optik **178**, 932–937 (2019).
17. T. H. Chow, K. M. Tan, B. K. Ng, S. G. Razul, C. M. Tay, T. F. Chia, and W. T. Poh, "Diagnosis of virus infection in orchid plants with high-resolution optical coherence tomography," J. Biomed. Opt.**14**, 14006 (2009).
18. T. Anna, S. Chakraborty, C.-Y. Cheng, V. Srivastava, A. Chiou, and W.-C. Kuo, "Elucidation of microstructural changes in leaves during senescence using spectral domain optical coherence tomography," Sci. Rep.**9**, 1167 (2019).
19. C. J. Larimer, E. H. Denis, J. D. Suter, and J. J. Moran, "Optical coherence tomography imaging of plant root growth in soil," Appl. Opt. **59**, 2474–2481 (2020).
20. M. Li, S. Landahl, A. R. East, P. Verboven, and L. A. Terry, "Optical coherence tomography—a review of the opportunities and challenges for postharvest quality evaluation," Postharvest Biol. Technol. **150**, 9–18 (2019).
21. P.-C. Cheng, "Interaction of light with botanical specimens," in *Handbook of Biological Confocal Microscopy*, J. B. Pawley, ed., 3rd ed. (Springer, 2006), pp. 414–441, Chap. 21.
22. G. R. Littlejohn, J. D. Gouveia, C. Edner, N. Smirnoff, and J. Love, "Perfluorodecalin enhances *in vivo* confocal microscopy resolution of *Arabidopsis thaliana* mesophyll," New Phytol.**186**, 1018–1025 (2010).
23. G. R. Littlejohn and J. Love, "A simple method for imaging *Arabidopsis* leaves using perfluorodecalin as an infiltrative imaging medium," J. Visual. Exp. **2**, 1 (2012).
24. P. J. de Wit and G. Spikman, "Evidence for the occurrence of race and cultivar-specific elicitors of necrosis in intercellular fluids of compatible interactions of *Cladosporium fulvum* and tomato," Physiol. Plant Pathol. **21**, 1–8 (1982).
25. J. Pfeifer, M. Mielewczik, M. Friedli, N. Kirchgessner, and A. Walter, "Non-destructive measurement of soybean leaf thickness via X-ray computed tomography allows the study of diel leaf growth rhythms in the third dimension," J. Plant Res. **131**, 111–124 (2018).
26. V. Coneva, M. H. Frank, M. A. D. L. Balaguer, M. Li, R. Sozzani, and D. H. Chitwood, "Genetic architecture and molecular networks underlying leaf thickness in desert-adapted tomato *Solanum pennellii*," Plant Physiol. **175**, 376 (2017).
27. J. Dupuis, C. Holst, and H. Kuhlmann, "Measuring leaf thickness with 3D close-up laser scanners: possible or not?" J. Imag. **3**, 22 (2017).
28. M. Wojtkowski, V. J. Srinivasan, T. H. Ko, J. G. Fujimoto, A. Kowalczyk, and J. S. Duker, "Ultrahigh-resolution, high-speed, fourier domain optical coherence tomography and methods for dispersion compensation," Opt. Express **12**, 2404–2422 (2004).
29. B. Baumann, C. W. Merkle, R. A. Leitgeb, M. Augustin, A. Wartak, M. Pircher, and C. K. Hitzenberger, "Signal averaging improves signal-to-noise in OCT images: But which approach works best, and when?" Biomed. Opt. Express**10**, 5755–5775 (2019).
30. U. Bechtold, J. N. Ferguson, and P. M. Mullineaux, "To defend or to grow: lessons from Arabidopsis C24," J. Exp. Botany**69**, 2809–2821 (2018).
31. G. J. Tearney, M. E. Brezinski, B. E. Bouma, M. R. Hee, J. F. Southern, and J. G. Fujimoto, "Determination of the refractive index of highly scattering human tissue by optical coherence tomography," Opt. Lett.**20**, 2258–2260 (1995).
32. J. Kalkman, A. V. Bykov, D. J. Faber, and T. G. van Leeuwen, "Multiple and dependent scattering effects in Doppler optical coherence tomography," Opt. Express**18**, 3883–3892 (2010).
33. K. F. Palmer and D. Williams, "Optical properties of water in the near infrared," J. Opt. Soc. Am.**64**, 1107–1110 (1974).
34. Q. Wu, X. Wang, L. Liu, and J. Mo, "Dual-side view optical coherence tomography for thickness measurement on opaque materials," Opt. Lett.**45**, 832–835 (2020).
35. T. Kawase, S. S. Sugano, T. Shimada, and I. Hara-Nishimura, "A direction-selective local-thresholding method, DSLT, in combination with a dye-based method for automated three-dimensional segmentation of cells and airspaces in developing leaves," The Plant J. **81**, 357–366 (2015).
36. G. W. Bassel and R. S. Smith, "Quantifying morphogenesis in plants in 4D," Curr. Opin. Plant Biol. **29**, 87–94 (2016).
37. R. Fernandez, P. Das, V. Mirabet, E. Moscardi, J. Traas, J. L. Verdeil, G. Malandain, and C. Godin, "Imaging plant growth in 4D: robust tissue reconstruction and lineaging at cell resolution," Nat. Methods**7**, 547–553 (2010).